Supplemental Online Material for "Quantum Mpemba effect without global symmetries"

Tanmay Bhore,[1] Lei Su,[2] Ivar Martin,[3,2] Aashish A. Clerk,[4] and Zlatko Papić[1]

[1] *School of Physics and Astronomy, University of Leeds, Leeds LS2 9JT, United Kingdom*
[2] *Department of Physics, University of Chicago, Chicago, Illinois 60637, USA*
[3] *Materials Science Division, Argonne National Laboratory, Lemont, Illinois 60439, USA*
[4] *Pritzker School of Molecular Engineering, University of Chicago, Chicago, Illinois 60637, USA*

(Dated: September 10, 2025)

In this Supplementary Material, we study several diagnostics of the quantum Mpemba effect (QME) and demonstrate that our choice of measure in the main text reproduces the previous results obtained using entanglement asymmetry in models with conserved U(1) charge. Furthermore, we support our conclusions in the main text for different types of initial states, including weakly-entangled states without translation invariance. Finally, we demonstrate that previous findings of "weak" and "strong" thermalization in the mixed field Ising model [1] can also be described in the framework of the QME.

ENTANGLEMENT ASYMMETRY AND TRACE DISTANCE

Most previous studies of the quantum Mpemba effect (QME) assumed models with a global symmetry, such as U(1), and the quantity dubbed "entanglement asymmetry" was introduced as a witness of the QME [2, 3]. Intuitively, entanglement asymmetry quantifies the restoration of symmetry in the reduced matrix describing a subsystem of the full system when the latter is quenched from an initial state that breaks the symmetry.

For a Hamiltonian with a global symmetry (assumed to be Abelian), consider a charge operator Q which may be decomposed as $Q = Q_A + Q_B$ for a given bipartitioning of the system. For any initial state ρ which commutes with Q, the reduction of ρ onto a subsystem by partial trace produces a density matrix that is block-diagonal in the basis of Q_A. Consider an initial state ρ which breaks the symmetry such that $[\rho, Q] \neq 0$. Then, at the level of the subsystem, $[\rho^A, Q_A] \neq 0$, implying that ρ^A is not a block-diagonal matrix in the basis of Q_A, but generally contains off-block-diagonal elements. The entanglement asymmetry is then defined as

$$\Delta S_A \equiv S(\rho^{A,Q}) - S(\rho^A), \quad S(\rho) = -\mathrm{Tr}(\rho \ln \rho), \quad \rho^{A,Q} = \sum_q \mathcal{P}_q \rho^A \mathcal{P}_q, \tag{1}$$

where $\mathcal{P}_q$ is a projector onto the eigenspace of Q_A with charge q. If $[\rho, Q] = 0$, then ρ^A is block-diagonal in the eigenbasis of Q_A and $S(\rho^{A,Q}) = S(\rho^A)$, thus the entanglement asymmetry vanishes, whereas $\Delta S_A > 0$ for a state that breaks the symmetry. Note that entanglement asymmetry can be written as a relative entropy: $\Delta S_A = S(\rho^A || \rho^{A,Q}) \equiv \mathrm{Tr}[\rho^A(\ln \rho^A - \ln \rho^{A,Q})]$.

The degree to which a state breaks the symmetry can be quantified by the norm of the commutator $[\rho, Q]$. Generally, we expect that if a state breaks the symmetry more, it will have a larger value of ΔS_A, making it a *bona fide* measure of symmetry breaking. In 1D short-range interacting systems, the Hohenberg-Mermin-Wagner theorem states that continuous symmetries, such as U(1), cannot be spontaneously broken at any finite temperature. This implies that a symmetry, which is broken initially, should be restored in thermal equilibrium, if thermal equilibrium is reached dynamically. Note that there are some known exceptions in systems with non-Abelian symmetries [4]. Furthermore, integrable or many-body localized systems do not thermalize. However, for "generic", non-disordered short-range interacting systems, we expect entanglement asymmetry to behave similarly to other measures of distance from thermal equilibrium [3].

In Fig. 1 we compare the trace distance of the initial reduced density matrix $\Delta(\rho_A)$, as defined in the main text, to the entanglement asymmetry ΔS_A in a chaotic short-ranged model with U(1) symmetry. We consider the XXZ Hamiltonian with next-nearest-neighbor couplings that break integrability, previously studied in Ref. [2]:

$$H = J_1 \sum_{i=1}^{N-1} \left(\sigma_i^x \sigma_{i+1}^x + \sigma_i^y \sigma_{i+1}^y + \Delta_1 \sigma_i^z \sigma_{i+1}^z\right) + J_2 \sum_{i=1}^{N-2} \left(\sigma_i^x \sigma_{i+2}^x + \sigma_i^y \sigma_{i+2}^y + \Delta_2 \sigma_i^z \sigma_{i+2}^z\right). \tag{2}$$

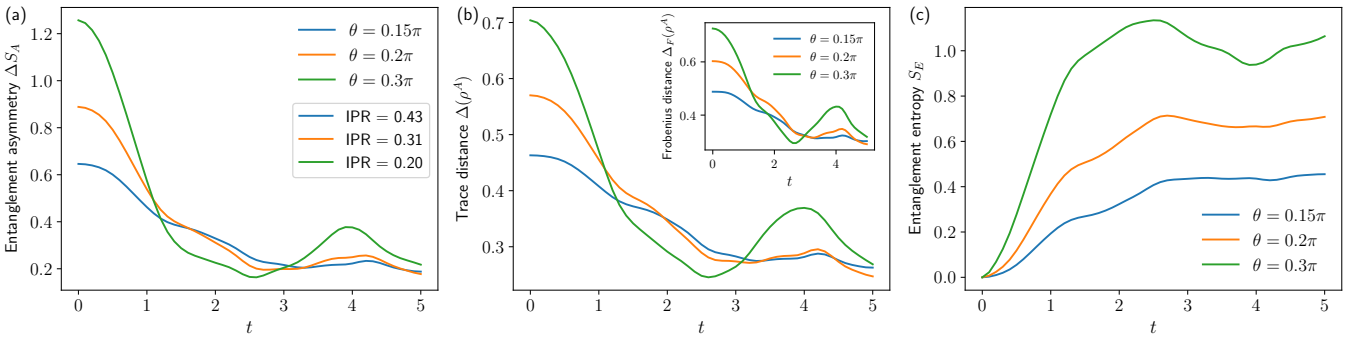

Figure 1. (a) Dynamics of entanglement asymmetry, (b) trace distance and Frobenius distance (inset) and (c) entanglement entropy for the chaotic XXZ model in Eq. (2) and ferromagnetic states in Eq. (3) tilted along the y-axis. Results are obtained by exact diagonalization for a system size $N = 10$ with $J_1 = J_2 = 1$ and $\Delta_1 = \Delta_2 = 0.5$.

This Hamiltonian has a U(1) symmetry as it conserves $M = \sum_i \sigma_i^z$; the initial breaking and restoration of this symmetry is measured by the entanglement asymmetry. Specifically, we consider tilted ferromagnetic states:

$$|\psi(\alpha;\theta)\rangle = \exp\left(-i\frac{\theta}{2}\sum_i \sigma_i^\alpha\right)|\uparrow\uparrow\uparrow ....\rangle\,,\ \alpha = x, y, z, \tag{3}$$

which break the U(1) symmetry for $\alpha = x, y$ and non-zero θ. We consider an equal bipartition of the system and calculate the entanglement asymmetry, trace and Frobenius distance (as defined in Eq. (4)) and the entanglement entropy for three different values of θ in Fig. 1. We observe that the trace and Frobenius distances qualitatively reproduce the behavior of the entanglement asymmetry and show the QME with increasing θ. This shows that the trace and Frobenius distance metrics used in the main text successfully captures the QME in systems with symmetries, considered in previous work.

We also find that the IPR of the states in Fig. 1 follows the expected trend as we observed in systems without symmetries in the main text, i.e., smaller IPR corresponding to a larger initial trace distance and simultaneously a faster rate of decay. Curiously, we also observe a difference in the slope of entanglement entropy, $S_E = -\mathrm{Tr}(\rho^A \ln \rho^A)$, for the same states. Although all three states have zero entanglement entropy initially, the states with slow trace distance dynamics also show slow growth and smaller saturation values of entanglement entropy. This also suggests a connection between the rate of entanglement entropy growth and the QME dynamics. We explore this connection further in the next section.

OTHER DIAGNOSTICS OF QME

Many possible metrics have been suggested to describe the QME dynamics, see Ref. [3] for a discussion. In the main text, we have employed the trace distance measure to compare the time-evolved density matrix with the diagonal ensemble. In contrast, recent experiments on trapped ions have characterized the QME dynamics using the Frobenius norm between the initial and the equilibrium density matrix [5]. Here, we confirm that the Frobenius norm qualitatively reproduces the QME dynamics as observed with the trace distance metric in the main text. The Frobenius distance of an initial state from the diagonal ensemble is defined as

$$\Delta_F(\rho^A) = \sqrt{1 - \min\left(1,\ \frac{2\,\mathrm{Tr}[\rho^A \rho^A_{\mathrm{DE}}]}{\mathrm{Tr}[(\rho^A)^2 + (\rho^A_{\mathrm{DE}})^2]}\right)}. \tag{4}$$

We consider $|\theta, \phi\rangle$ initial states defined in the main text and evaluate the initial Frobenius distance across the full range of θ, ϕ values in Fig 2(a). The Frobenius distance metric behaves similarly to the trace distance metric in Fig. 2 of the main text. We also consider states of Type 1, marked by stars in Fig 2(a), and calculate the dynamics of their Frobenius distance in Fig 2(b). Similar to the results in the main text, we find the QME dynamics in the Frobenius distance as θ is increased, pointing to its robustness against the choice of distance metrics.

Given the crucial role of energy distributions on the QME dynamics, it is natural to ask if other measures of the energy distribution could act as reliable metrics of the QME. Here, we show that one of the simplest alternative

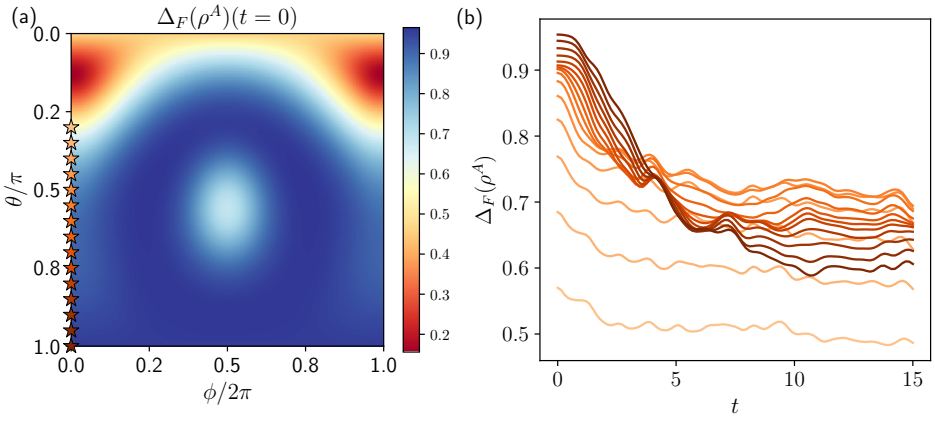

Figure 2. (a) Frobenius distance of tilted ferromagnetic states from the diagonal ensemble, reduced to a subsystem A of $N/2$ sites in the mixed field Ising model. (b) Dynamics of the Frobenius distance for Type 1 initial states marked by stars in panel (a). Results are for system size $N = 10$ obtained by exact diagonalization.

measures – the energy variance of initial states – does not act as a good metric of the QME dynamics. First, the average energy of the $|\theta, \phi\rangle$ states in Eq. (2) for the mixed field Ising Hamiltonian admits a simple form and is given by

$$\lim_{N\to\infty} \langle \hat{H}_{\rm MFIM}\rangle_{|\theta,\phi\rangle}/N = J_{zz}\cos^2(\theta) + h_x \sin(\theta)\cos(\phi) + h_z\cos(\theta). \tag{5}$$

We use the standard definition of the energy variance:

$$var(H) \equiv \langle \hat{H}^2\rangle_\Psi - \langle \hat{H}\rangle_\Psi^2. \tag{6}$$

In Fig. (3)(a)-(b), we plot the IPR and the energy variance, $var(H)$, for the $|\theta, \phi\rangle$ states of Eq. (2) of the main text for the mixed field Ising Hamiltonian in Eq. (1). For the states of Type 1 and 2, considered in Fig. 1 of the main text, the IPR either decreases monotonically (Type 1) or stays constant (Type 2), whereas their energy variance shows no such correlation. This indicates that the energy variance does not act as a sensitive metric of the QME dynamics for the models considered in this paper.

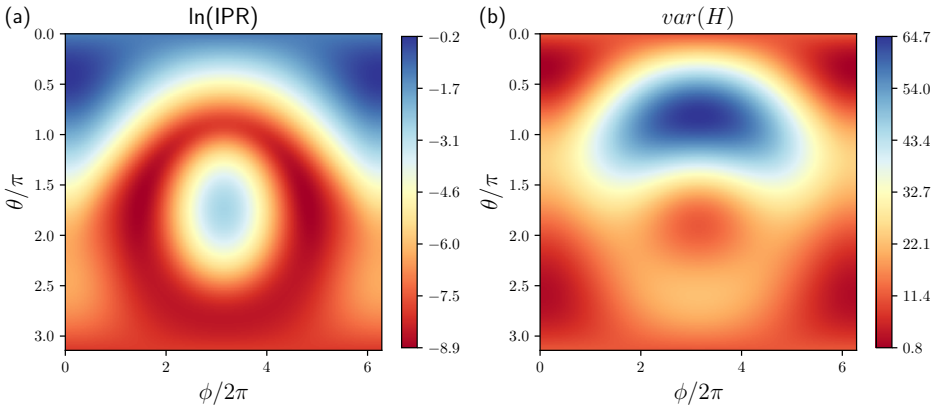

Figure 3. (a) IPR and (b) energy variance of the $|\theta, \phi\rangle$ states for the mixed field Ising Hamiltonian in the main text. Unlike the IPR, the energy variance does not capture the states associated with the QME dynamics observed in Fig. 1 of the main text. Results are obtained by exact diagonalization for the system size $N = 14$.

Indeed, it can be argued that energy variance and IPR do not necessarily imply the same thing. The IPR quantifies delocalization over *eigenstates*, and it is high (low) if the state is more localized (delocalized) over the energy eigenbasis. On the other hand, the energy variance, measuring how sharply peaked the energy distribution is around its mean, is high (low) if the energy distribution is broad (sharp). Naively, one might expect states with high energy variance

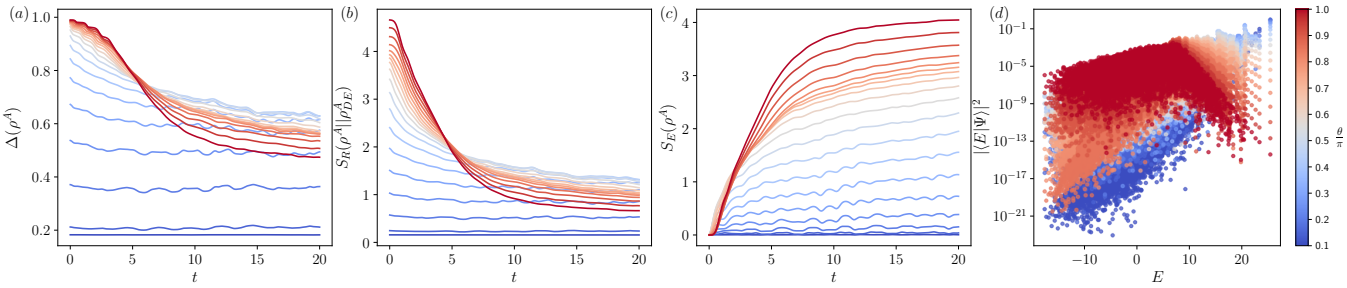

Figure 4. Dynamics of trace distance (a), relative entropy (b) and entanglement entropy (c), with energy distributions of the initial states (d). All data is for the mixed field Ising Hamiltonian from the main text and tilted ferromagnetic states in Eq. (2). System size is $N = 14$ with a subsystem size of 7 sites.

to have a low IPR and vice versa. To see why this need not always be the case, consider a state that is delocalized over an extensive number of eigenstates that all have nearly the same energy. Then, the IPR of the state is low, whereas the energy variance is small, as the energies are tightly clustered. Conversely, if the state is delocalized over two energy eigenstates with very different energies, the IPR is high but the energy variance is also large. Thus, the two quantities probe fundamentally different aspects of the energy distribution.

While energy variance is insufficient to explain our results, we are able to draw connections with another standard measure of thermalization: the growth of entanglement entropy. Although infinite temperature states in chaotic quantum systems are expected to show ballistic growth of entanglement [6], the rate of growth can depend finely on the temperature of the initial states. Since the QME dynamics observed for states of Type 1 in the mixed field Ising model in the main text relies on varying the temperature of initial states, we expect to see this reflected in the rate of growth of entanglement entropy. We consider two entropic quantities; the entanglement entropy S_E and the relative entropy of the state with its diagonal ensemble, $S_R(\rho^A||\rho^A_{\rm DE}) = {\rm Tr}[\rho^A(\ln\rho^A - \ln\rho^A_{\rm DE})]$, where $\rho^A_{\rm DE}$ is the diagonal ensemble for ρ reduced to subsystem A. We consider states in Eq. (3) tilted around the y-axis and evolve them under the mixed field Ising Hamiltonian in the main text. The trace distance $\Delta(\rho^A)$, relative entropy S_R and entanglement entropy S_E for varying θ are shown in Fig 4(a)-(c). We observe that both the trace distance and the relative entropy capture the QME dynamics, with eventual crossings appearing as θ is increased. This growth is supplemented by the dynamics of entanglement entropy, where we observe an increasing rate of growth and saturation value of entropy as θ is increased. Increasing θ increases the effective temperature of the state and we expect the fastest growth and saturation to the Page value of entropy at infinite temperature [7].

To gain a finer understanding of these results, we also look at the energy eigenstate overlaps of these initial states, shown in Fig 4(d). For small θ, the initial state has the largest overlap on the most excited eigenstate. With increasing θ, the weight of the initial state on the most excited state consistently decreases, while the spectrum simultaneously flattens. This delocalization is marked by the monotonic decrease in IPR values, as previously seen in Fig. 2 of the main text.

FINITE-SIZE SCALING OF TRACE DISTANCE DYNAMICS

In this section, we perform a system-size scaling analysis of the trace distance dynamics for Type 1, i.e., tilted ferromagnetic initial states in the mixed field Ising model of Eq. (1) in the main text. This scaling can be performed in two complementary ways, either by fixing the total system size N and increasing the subsystem size N_A up to the maximum of $N/2$, or by keeping N_A fixed and scaling up N. The latter method gives us a way to access properties of a finite subsystem in the thermodynamic limit. At first, we fix the total system size to $N = 14$ and consider the first N_A spins from the left as our subsystem. The corresponding trace distance dynamics as N_A is varied from 1 to 6 is shown in Fig. 5. Thermalization in isolated systems requires that the size of the bath be much bigger than the subsystem size for the subsystem to effectively thermalize. This is evident in Fig. 5; for small N_A, the effective bath is much larger than the subsystem and the trace distance $\Delta(\rho^A)$ drops close to zero for most initial states, whereas upon increasing the size of the subsystem, the trace distance plateaus further away from zero. However, QME is visible for all choices of N_A.

Next, we plot the scaling of saturation values of the trace distance for a fixed subsystem size, $N_A = 4$ as a function of N in Fig. 6. For small θ, the states remain close to the edge of the spectrum and the trace distance does not go

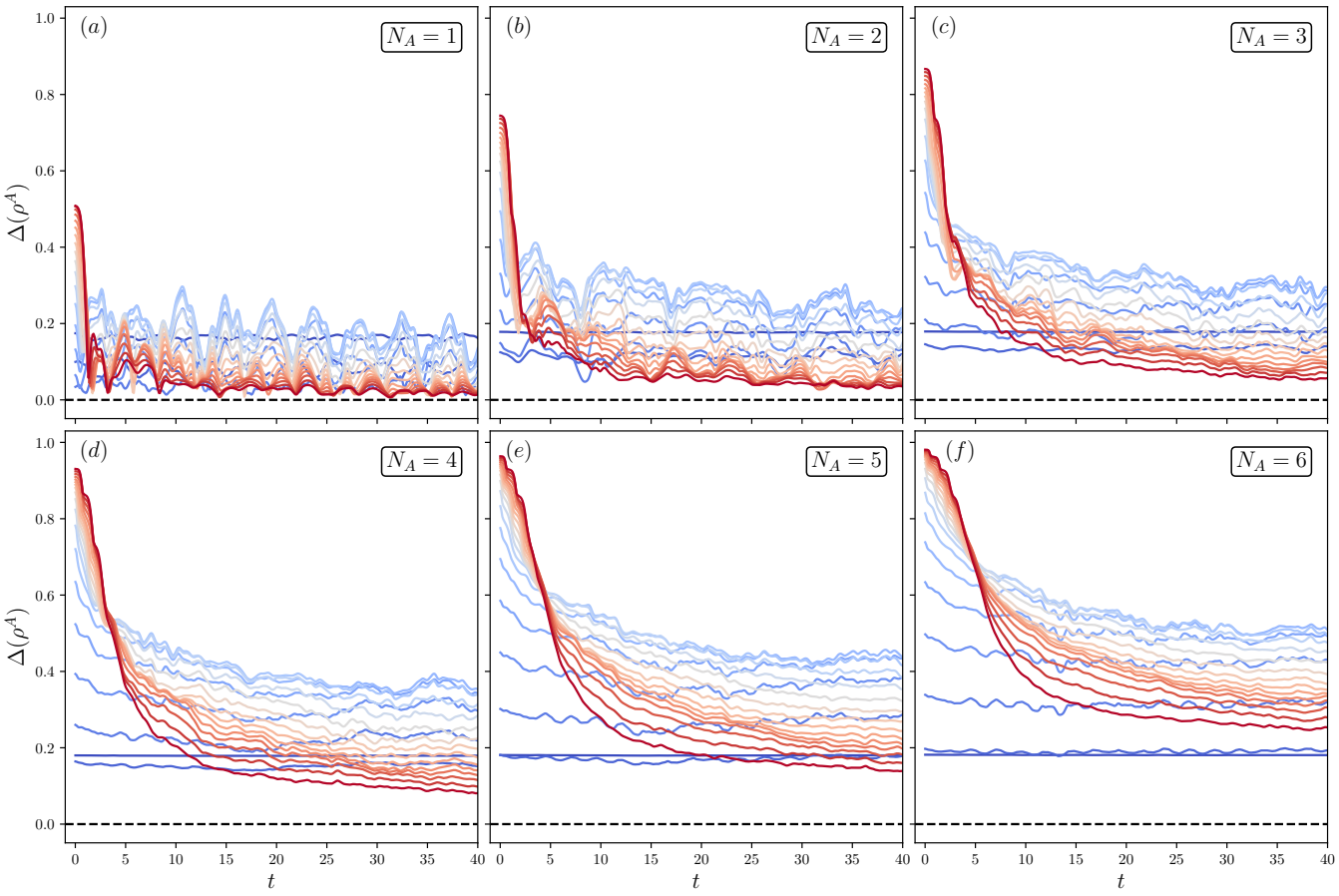

Figure 5. Trace distance dynamics of Type 1 initial states in the mixed field Ising model for increasing size of the subsystem A. The system size is $N = 14$ and the subsystem is chosen as the first N_A spins from the left.

to zero with increasing N, whereas it drops to zero exponentially with N for large θ as the states delocalize over the energy eigenbasis.

OTHER INITIAL STATES

In the main text we have focused on two classes of translation-invariant product states: Type 1 states with increasing energies (effective temperature) and Type 2 states at a fixed energy or effective temperature. Given the correlation between IPR values and the initial tace distance in Fig. 2 of the main text, we expect to see the QME dynamics across a large range of θ, ϕ values, so long as we stay away from the boundaries of the spectrum. Here, we give two examples of states progressively rotated around the $\hat{z}$ axis on the Bloch sphere by varying ϕ for two fixed values of θ. The states are marked by the orange and green stars in Fig 7(a). Both sets of states show progressively increasing energies/effective temperatures. Their trace distance dynamics, obtained by time evolution under the mixed field Ising Hamiltonian of Eq. (1) of the main text, is plotted in Fig 7(b)-(c). This shows the QME as ϕ is increased, whereas the IPR of the states progressively decreases with ϕ (inset), consistent with the results for Type 1 and 2 states in the main text. Since the IPR is anti-correlated with the initial trace distance, we expect to see the QME for *any* two choices of θ, ϕ in this model, as long as we are away from the edges of the spectrum.

For the time-independent Hamiltonians considered in the main text, we have focused on product states to demonstrate the QME, however, weakly-entangled initial states were required to observe the QME in the Floquet model. This raises the question: is the QME for time-independent Hamiltonians also sensitive to the entanglement in the initial state? Moreover, does the IPR remain a faithful criterion for weakly-entangled initial states? Here, we answer this question by looking at the dynamics of the mixed field Ising model in Eq. (1) of the main text for weakly entangled initial states. We consider ferromagnetic states tilted around the y-axis, as defined in Eq (3) for $\alpha = y$. We entangle

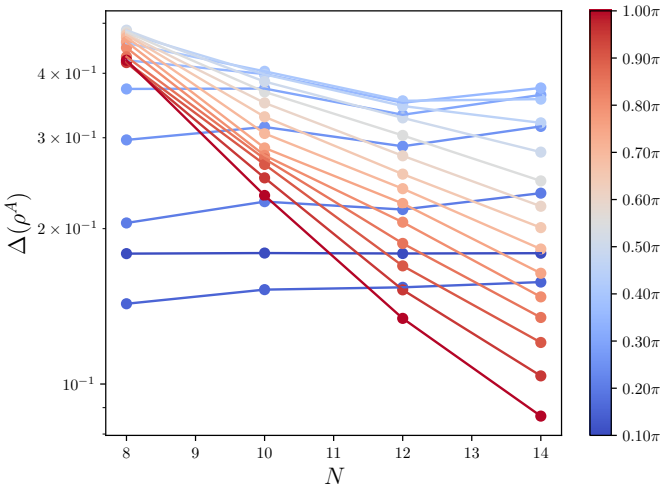

Figure 6. Saturation value of trace distance of Type 1 initial states in the mixed field Ising model with a fixed subsystem size $N_A = 4$ and increasing total system size N. While the saturation value plateaus with system size for small θ, it drops to zero exponentially with N for large θ.

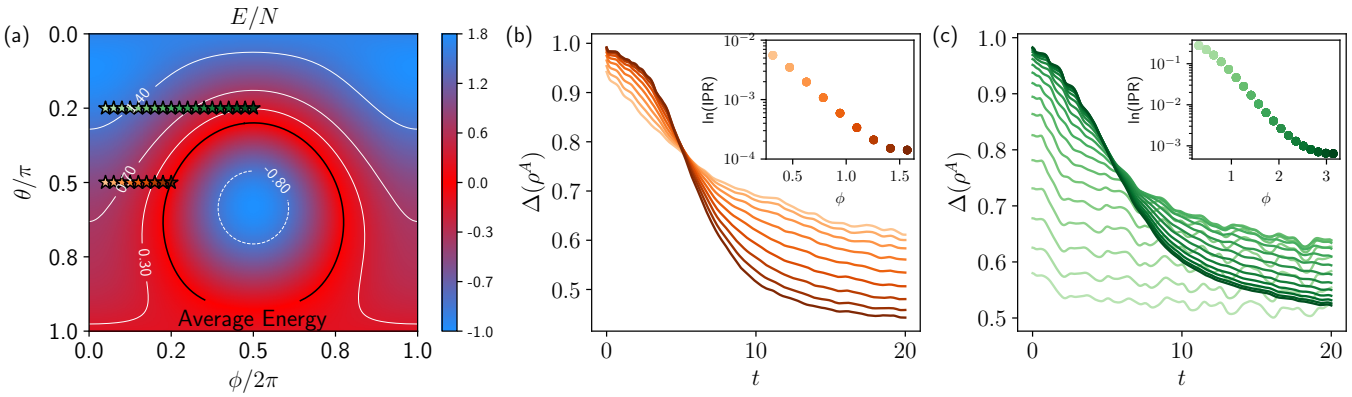

Figure 7. (a) Energy density of $|\theta, \phi\rangle$ states on the Bloch sphere along with two classes of states marked with orange and green stars. (b)-(c) Trace distance dynamics of the states marked by orange and green along with their IPRs(inset). The QME is visible in both the cases. Results are shown for $N = 14$.

these initial states through the action of a local unitary operator of the form $e^{-i\delta t \hat{H}_R}$, where $\hat{H}_R = \sum_i \hat{h}_i$, and each $\hat{h}_i$ is a Haar-random operator defined on two sites. After a random evolution up to time δt, we evolve the resulting states with the mixed field Ising Hamiltonian in Eq. (1) of the main text. The resulting dynamics of the subsystem trace distance, entanglement entropy, overlaps with energy eigenstates and the IPR are shown in Fig. 8 for $\delta t = 0.2, 0.3, 0.5$. For a small δt, the initial states are weakly entangled and the QME is visible with a large variation in the dynamics and energy distributions. With increasing δt, the initial states are "homogenized" by the random Hamiltonian leading to almost identical dynamics, thus the QME is absent. Thus, the IPR correlates with the QME for weakly-entangled initial states, even for states that break translation invariance.

QME WITH A FIXED INITIAL STATE

The conventional setup of the QME consists of a fixed Hamiltonian and varying initial states. Here, we consider an alternative setup with a fixed initial state that is quenched using different Hamiltonians, leading to the QME. We exemplify this using the random Hamiltonian in Eq. (7) of the main text, where the three components $\mathbf{v}_i = (v_x, v_y, v_z)_i$ are real numbers drawn uniformly from the window $[-W, W]$ and $J_{\rm H}$ is kept uniform and controls the strength of the Heisenberg term. We fix the initial state to be the ferromagnetic state $|\text{FM}\rangle \equiv |\theta = 0, \phi\rangle$ in Eq. (1) of the main text.

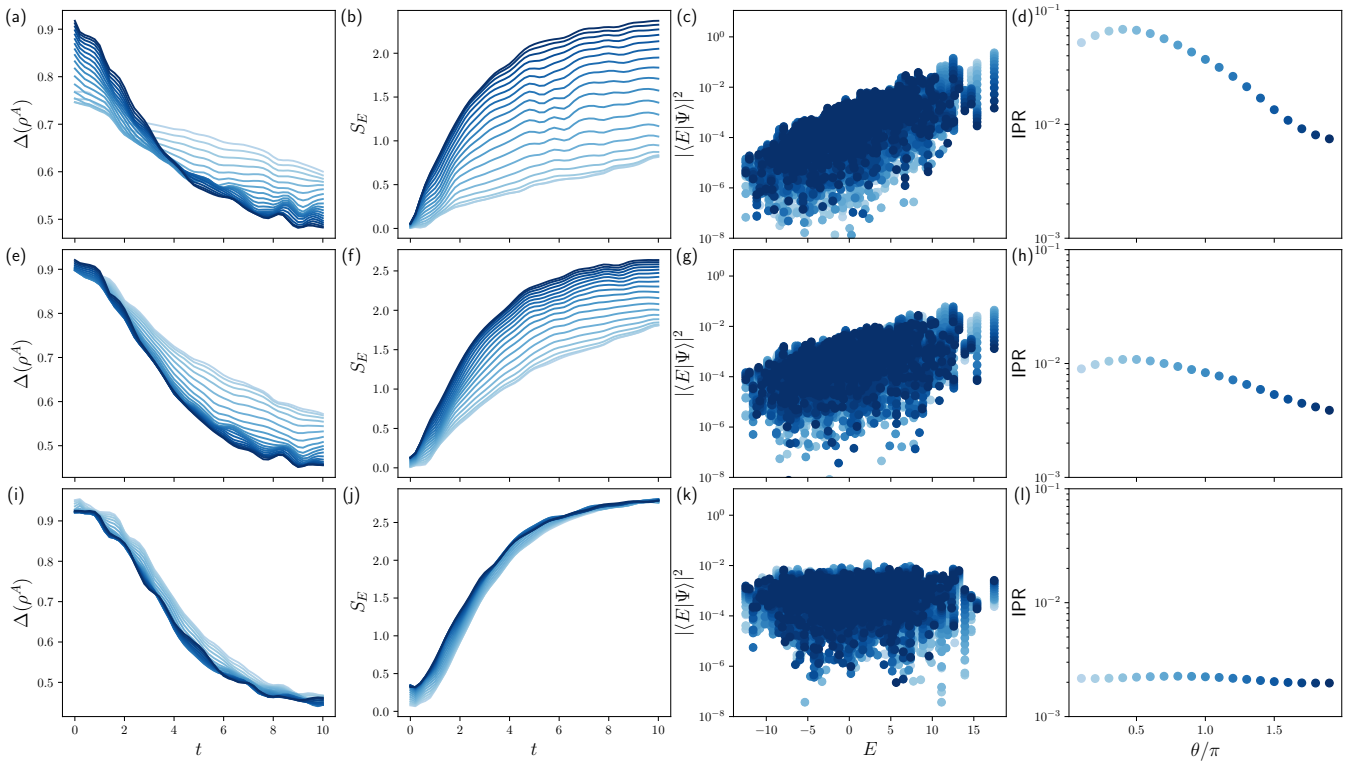

Figure 8. QME for weakly entangled initial states in the mixed field Ising model. Trace distance dynamics, entanglement entropy dynamics, overlaps with energy eigenstates and IPR of initial states which undergo random entangling evolution for $\delta t = 0.2$ (a)-(d), $\delta t = 0.3$ (e)-(h) and $\delta t = 0.5$ (i)-(l). All data is for system size $N = 10$ obtained by exact diagonalization.

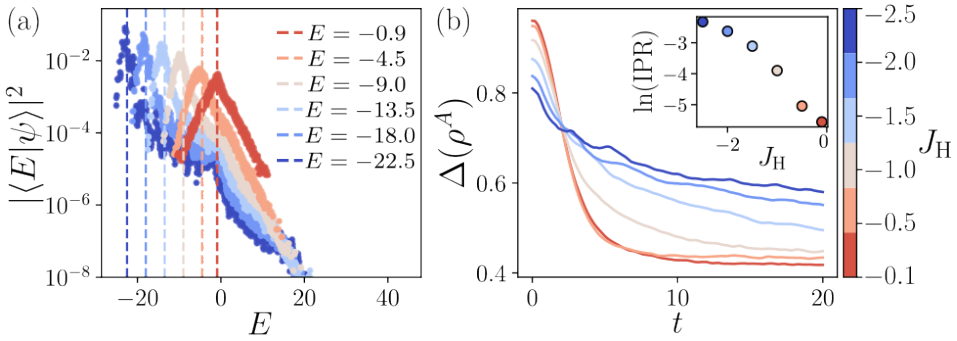

Figure 9. QME in the random model, Eq. (7) of the main text, with a fixed initial state $|\mathrm{FM}\rangle \equiv |\theta = 0, \phi\rangle$. (a) Averaged overlaps of $|\mathrm{FM}\rangle$ state with energy eigenstates as a function of their energy. Different colors represent different values of J_H [denoted in the legend of panel (b)], which translate into the average values of the energy quoted in the legend. (b) Trace distance dynamics for the $|\mathrm{FM}\rangle$ state and different values of J_H, with the corresponding IPR values given in the inset. The crossing associated with the QME is visible as the effective temperature of the state is tuned by deforming the Hamiltonian. The inset shows the IPR for the same states as a function of f. All data is for the system size $N = 10$ and fixed disorder window $W = 1$.

Any local term of the form $(\boldsymbol{\sigma}_i \times \boldsymbol{\sigma}_{i+1}) \cdot \hat{\mathbf{v}}$ has a zero expectation value for $|\mathrm{FM}\rangle$, making $|\mathrm{FM}\rangle$ an infinite temperature state for such Hamiltonians. We tune the energy density of $|\mathrm{FM}\rangle$ via the strength of J_H of the Heisenberg term.

In Fig. 9(a), we show the overlaps of $|\mathrm{FM}\rangle$ with energy eigenstates of H_R, for a few choices of J_H and each averaged over 50 random realizations. For large negative J_H, the overlap peaks near the ground state, and in the limit $J_\mathrm{H} \to -\infty$, $|\mathrm{FM}\rangle$ becomes the ground state of H_R. As J_H increases toward zero, the overlap peak shifts to the middle of the spectrum, moving the state toward infinite temperature. This coincides with a flattening of the distribution, as reflected in the decreasing IPR shown in the inset of Fig. 9(b), marking delocalization over a larger

number of eigenstates. Indeed, QME is evident in the trace distance dynamics in Fig. 9(b), where increasing $J_{\rm H}$ leads simultaneously to higher initial $\Delta(\rho^A)$ values and faster decay rates, resulting in a crossing.

STRONG VS. WEAK THERMALIZATION AS A FORM OF THE QME

Differences in the rate of thermalization of product states in non-integrable models, dubbed "strong" and "weak" thermalization, were noted in Ref. [1] predating recent QME developments. Here, we argue that the results of Ref. [1] can be interpreted as a manifestation of the QME dynamics, which can be explained by the simple criteria based on energy distributions introduced in the main text.

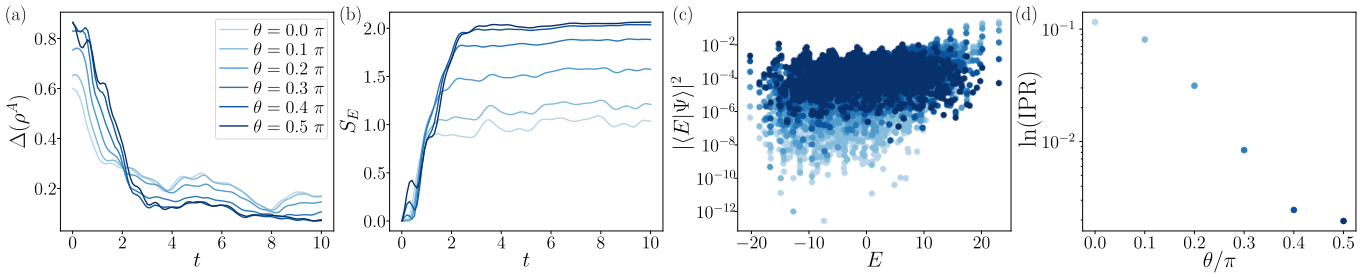

Figure 10. Strong vs. weak thermalization in the mixed field Ising model [1] as a manifestation of the QME. We consider ferromagnetic states in Eq. (3) rotated about the x-axis. (a) Trace distance dynamics. (b) Entanglement entropy dynamics. (c) Overlaps with energy eigenstates. (d) IPR as a function of tilt angle θ. Data is for system size $N = 10$ obtained by exact diagonalization.

We consider the same mixed field Ising model as in the main text and set the field strengths to $(J_{zz}, h_x, h_z) = (1, -1.5, 0.5)$, as done in Ref. [1] (see also Ref. [8]). Excluding the additional boundary terms, the Hamiltonian has a reflection symmetry about the center of the chain, which we resolve by restricting the Hilbert space to states with parity $+1$. As an example of a strongly-thermalizing state, Ref. [1] considered the product state of spins polarized along the y-axis, which is effectively at infinite temperature $\beta = 0$. On the other hand, an example of a "weakly-thermalizing" state was the product state of spins pointing along the z-direction, whose effective temperature is $\beta \approx 0.7275$. In Fig. 10 we demonstrate that these two states are associated with the QME. We can tune between them by taking the ferromagnetic states in Eq. (3) and performing the rotation by an angle θ around the $\hat{x}$-axis, with the two states recovered in the limits $\theta = 0$ and $\theta = \pi/2$. We fix the subsystem A to be the central 3 sites of the chain and calculate the trace distance dynamics, entanglement entropy, overlaps with energy eigenstates and the IPR in Fig. 10. Upon increasing θ, QME dynamics is evident the initial trace distance and its rate of decay increases simultaneously, accompanied by an increasing growth rate and saturation value of entanglement entropy. We observe that the IPR of these states also steadily decreases with increasing θ, consistent with other results in the main text.

[1] M. C. Bañuls, J. I. Cirac, and M. B. Hastings, Strong and weak thermalization of infinite nonintegrable quantum systems, Phys. Rev. Lett. **106**, 050405 (2011).
[2] F. Ares, S. Murciano, and P. Calabrese, Entanglement asymmetry as a probe of symmetry breaking, Nat. Commun. **14** (2023).
[3] F. Ares, P. Calabrese, and S. Murciano, The quantum Mpemba effects, arXiv:2502.08087 (2025).
[4] F. Ares, S. Murciano, E. Vernier, and P. Calabrese, Lack of symmetry restoration after a quantum quench: An entanglement asymmetry study, SciPost Phys. **15**, 089 (2023).
[5] L. K. Joshi, J. Franke, A. Rath, F. Ares, S. Murciano, F. Kranzl, R. Blatt, P. Zoller, B. Vermersch, P. Calabrese, C. F. Roos, and M. K. Joshi, Observing the quantum Mpemba effect in quantum simulations, Phys. Rev. Lett. **133**, 010402 (2024).
[6] H. Kim and D. A. Huse, Ballistic spreading of entanglement in a diffusive nonintegrable system, Phys. Rev. Lett. **111**, 127205 (2013).
[7] D. N. Page, Average entropy of a subsystem, Phys. Rev. Lett. **71**, 1291 (1993).
[8] I. A. Maceira and A. M. Läuchli, Thermalization dynamics in closed quantum many body systems: a precision large scale exact diagonalization study, arXiv:2409.18863 (2024).